ORGANOMETALLICS

Experimental and Computational Studies of the Single-Molecule Conductance of Ru(II) and Pt(II) *trans*-Bis(acetylide) Complexes

Oday A. Al-Owaedi,[†,‡,#] David C. Milan,[§,#] Marie-Christine Oerthel,[∥,#] Sören Bock,[⊥] Dmitry S. Yufit,[∥] Judith A. K. Howard,[∥] Simon J. Higgins,[§] Richard J. Nichols,*[,§] Colin J. Lambert,*[,†] Martin R. Bryce,*[,∥] and Paul J. Low*[,⊥]

[†]Department of Physics, University of Lancaster, Lancaster LA1 4YB, U.K.
[‡]Department of Laser Physics, Women Faculty of Science, Babylon University, Hilla, Iraq
[§]Department of Chemistry, University of Liverpool, Crown Street, Liverpool L69 7ZD, U.K.
[∥]Department of Chemistry, Durham University, South Road, Durham DH1 3LE, U.K.
[⊥]School of Chemistry and Biochemistry, University of Western Australia, 35 Stirling Highway, Crawley, Perth 6009, Australia

S *Supporting Information*

ABSTRACT: The single-molecule conductance of metal complexes of the general forms *trans*-Ru(C≡CArC≡CY)$_2$(dppe)$_2$ and *trans*-Pt(C≡CArC≡CY)$_2$(PPh$_3$)$_2$ (Ar = 1,4-C$_6$H$_2$-2,5-(OC$_6$H$_{13}$)$_2$; Y = 4-C$_5$H$_4$N, 4-C$_6$H$_4$SMe) have been determined using the STM $I(s)$ technique. The complexes display high conductance (Y = 4-C$_5$H$_4$N, M = Ru (0.4 ± 0.18 nS), Pt (0.8 ± 0.5 nS); Y = 4-C$_6$H$_5$SMe, M = Ru (1.4 ± 0.4 nS), Pt (1.8 ± 0.6 nS)) for molecular structures of ca. 3 nm in length, which has been attributed to transport processes arising from tunneling through the tails of LUMO states.
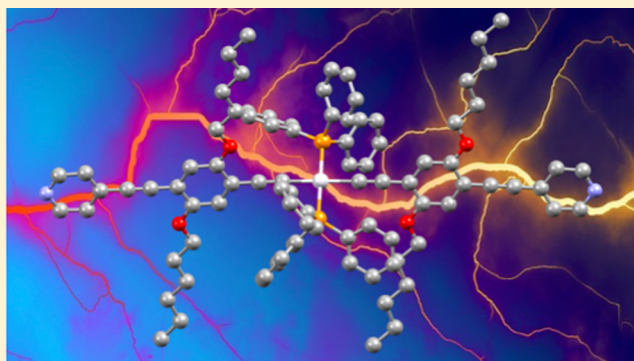
INTRODUCTION

Measurements of the electrical characteristics of a wide variety of saturated, conjugated, and redox-active organic compounds have served to drive the development of concepts and techniques in molecular electronics.[1−3] However, metal complexes offer several potential advantages over organic compounds as components in molecular electronic devices, including redox activity at moderate potentials, ready tuning of frontier molecular orbital energy levels to better match the Fermi levels of metallic electrodes, and magnetic properties.[4,5] Consequently, attention has been turned to the construction and study of metal complexes,[6−14] clusters,[15−18] extended metal atom chains,[19−21] and organometallic acetylide species[22−34] within molecular junctions.

In the case of purely organic oligo(aryleneethynylene)-based compounds with pyridyl contacting groups, the molecular conductance, as determined by single-molecule STM break junction (STM-BJ) experiments, decreases with length, initially in line with the exponential decay expected for a tunneling mechanism before shifting to a shallower length dependence more indicative of an incoherent hopping mechanism of charge transport for compounds of ca. 3 nm in length.[35] Conductance values range from $10^{-4.5}G_0$ (2.45 nS) for the 1.6 nm long "three-ring" oligoarylenes NH$_4$C$_5$C≡CC$_6$H$_2$R$_2$C≡CC$_5$H$_4$N (R = OC$_6$H$_{13}$), decreasing by approximately 3 orders of

magnitude for the 3.0 nm long "five-ring" system NH$_4$C$_5$C≡C(C$_6$H$_2$R$_2$C≡C)$_3$C$_5$H$_4$N ($10^{-6.7}G_0$, 0.015 nS), and thereafter falling only slightly to $10^{-6.9}G_0$ (0.01 nS) in an analogous 5.8 nm long "nine-ring" system.

In cases where direct comparison is possible, it has generally been found that the incorporation of a ruthenium metal center such as Ru(dppm)$_2$[34] or Ru(dppe)$_2$[29] within a π-conjugated wirelike structure leads to a 2−5-fold increase in conductance with the conductance value measured likely also being dependent on the nature of the molecule−electrode contacting group (e.g., *trans*-Ru(C≡CC$_6$H$_4$SAc)$_2$(dppm)$_2$, STM break junction 19 ± 7 nS;[34] *trans*-Ru(C≡CC$_6$H$_4$C≡C-SiMe$_3$)$_2$(dppe)$_2$, $I(s)$ method [(5.1 ± 0.99) × 10^{-5}]G_0/3.9 ± 0.8 nS;[29] *trans*-Ru(C≡C-4-C$_5$H$_4$N)$_2$(dppe)$_2$, STM-BJ [(2.5 ± 0.4) × 10^{-4}]G_0/19 ± 3 nS[28]).

In contrast, earlier studies have shown that the Pt(II) complex *trans*-Pt(C≡CC$_6$H$_4$SAc)$_2$(PPh$_3$)$_2$ behaves rather more as an insulating species when it is bound within a mechanically controlled break junction (MCBJ), with resistances (5−50 GΩ; 0.2−0.02 nS) some 3 orders of magnitude larger than those of the comparable organic compounds AcSC$_6$H$_4$C≡CArC≡CC$_6$H$_4$SAc (Ar = 9,10-C$_{14}$H$_8$, 1,4-C$_6$H$_2$-

2-NH$_2$-5-NO$_2$) being reported.[22] A later study with a range of *trans*-Pt(C≡CC$_6$H$_4$SAc)$_2$(PR$_3$)$_2$ complexes (R = Cy, Ph, OEt) revealed little effect of the supporting phosphine or phosphite ligand on the through-molecule conductance, although curiously the conductance for these Pt complexes measured in a cross-wire junction was reported to be some 2−3-fold greater than that of the simple oligo(phenyleneethynylene) AcSC$_6$H$_4$C≡CC$_6$H$_4$C≡CC$_6$H$_4$SAc.[23]

Here we turn our attention to a family of linearly conjugated, wirelike organometallic complexes featuring *trans*-Ru(C≡CR)$_2$(dppe)$_2$ and Pt(C≡CR)$_2$(PPh$_3$)$_2$ moieties embedded within the oligo(aryleneethynylene) backbone of ca. 3 nm molecular length and describe the results of single-molecule conductance studies based on the $I(s)$ method. These metal complexes are substantially more conductive than their purely organic analogues of comparable molecular length, with detailed computational investigation indicating that the enhanced conductance arises from conductance through the tails of the LUMO resonances. The conductance values obtained from the Pt and Ru systems are remarkably similar, suggesting that the readily synthesized platinum complexes may have an important role to play in the further development of metal complexes for applications in single-molecule electronics.

■ RESULTS AND DISCUSSION

Single-molecule measurements using both organic and organometallic compounds have clearly shown that the electronic properties of the prototypical metal|molecule|metal junctions not only are strongly influenced by the chemical structure of the molecular backbone but also are critically dependent on the combination of the surface and contacting groups.[36−43] The pyridyl-terminated compounds **1-Ru** and **1-Pt** together with the analogous methyl thioether terminated compounds **2-Ru** and **2-Pt** were chosen to explore both the relative effects of the Ru(dppe) vs Pt(PPh$_3$)$_2$ fragments on molecular conductance and the influence of the electrode−molecule contact in a comparable set of compounds (Scheme 1). The pyridyl and methyl thioether moieties are already established as surface-contacting groups in single-molecule studies of oligoynes and oligo(phenyleneethynylenes).[9,35,37,44−47]

The complexes **1-Ru**, **1-Pt**, **2-Ru**, and **2-Pt** were synthesized in a convergent fashion as indicated in Scheme 1. The precursor terminal alkynyl complexes were assembled from the protected ligand building block 2-((triisopropylsilyl)ethynyl)-5-ethynyl-1,4-bis(hexyloxy)benzene and [RuCl(dppe)$_2$]OTf, via a sequence of intermediate vinylidene species which were not isolated but deprotonated in situ, or PtCl$_2$(PPh$_3$)$_2$, through simple CuI-catalyzed alkynylation reactions in diethylamine. After removal of the triisopropylsilyl protecting group, the surface binding groups were readily introduced by the "on-complex" cross-coupling reactions with 4-iodopyridine or 4-iodothioanisole (Scheme 1).

The STM $I(s)$ technique was used to measure the single-molecule conductance of the series of compounds **1-M** and **2-M** (M = Ru, Pt) in mesitylene solution, with a flame-annealed Au(111) gold-on-glass substrate serving as the bottom electrode and the STM tip creating the top electrode in these elementary metal|molecule|metal junctions. The current is recorded at a fixed bias, while the junction is elongated by retraction of the STM tip to generate conductance traces.[48] From analyses of the conductance traces, break-off distances of 3.1 nm (**1-Ru**) and 3.0 nm (**1-Pt**) can be determined (Table 1). The break-off distances quoted correspond to 95th percentile

Scheme 1. Synthesis of 1-Ru, 1-Pt, 2-Ru, and 2-Pt[a]
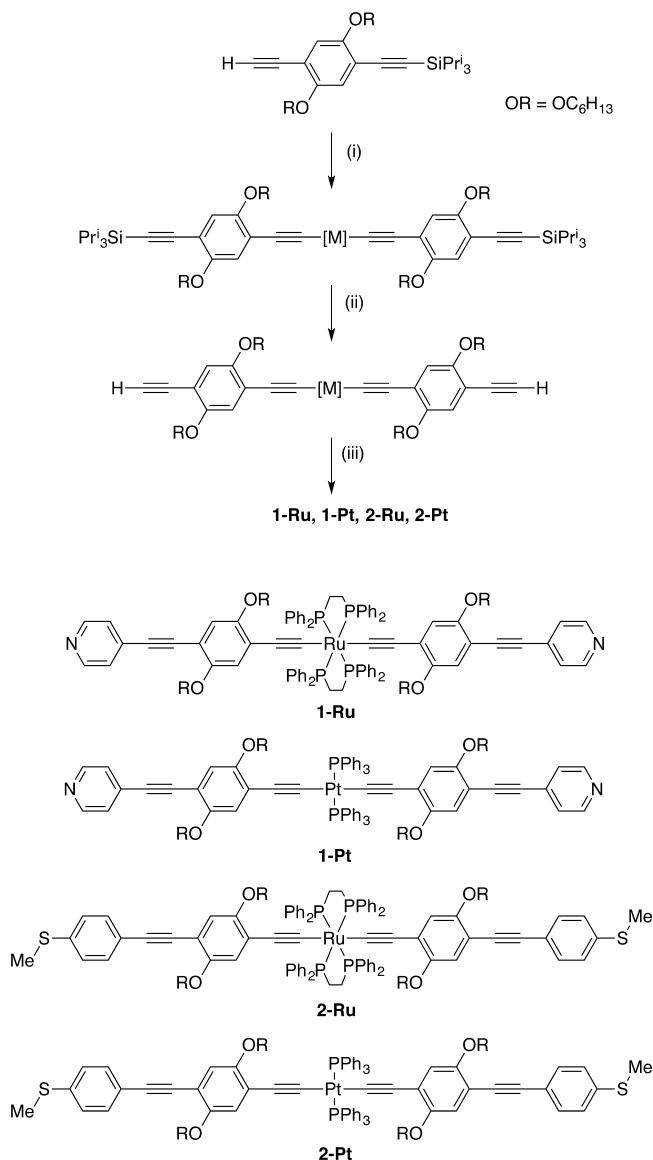
[a]Reagents and conditions: (i) (a) [RuCl(dppe)]OTf/DBU, (b) TlBF$_4$ (76%) or (a) *cis*-PtCl$_2$(PPh$_3$)$_2$/CuI(cat)/NHEt$_2$ (81%); (ii) NBu$_4$F ([M] = Ru(dppe)$_2$, 60%; [M] = Pt(PPh$_3$)$_2$, 63%); (iii) 4-iodopyridine/Pd(PPh$_3$)$_4$/CuI (cat.)/NEt$_3$ (**1-Ru**, 64%; **1-Pt**, 30%) or 4-iodothioanisole/Pd(PPh$_3$)$_4$/CuI (cat.)/NEt$_3$ (**2-Ru**, 34%; **2-Pt**, 17%).

values from the accumulated $I(s)$ scans. These values compare well with the N···N distance obtained from single-crystal X-ray diffraction studies of **1-Ru** (Figure 1, 2.86 nm) and **1-Pt** (Figure 2, 2.86 nm), noting that in the solid state these compounds are not perfectly linear but rather exhibit sigmoidal (**1-Ru**) or gracefully curved (**1-Pt**) structures arising from crystal-packing effects. Nevertheless, the good agreement between the break-off distance and the calculated molecular lengths (vide infra) is consistent with the contact of these molecules almost normal to the electrode surface via the pyridine lone pair within these molecular junctions.

In contrast, shorter break-off distances are determined for the methyl thioether complexes **2-Ru** (2.4 nm) and **2-Pt** (2.5 nm); cf. the S···S distance of 3.18 nm in the crystallographically determined molecular structure from a weakly diffracting

Table 1. Frontier Orbital Energies (eV), Experimental (exp G/G_0) and Calculated (th G/G_0) Conductances at $E_F - E_F^{DFT} = -0.07$ eV, Experimental 95th Percentile Break-off Distance Z^* (nm), Molecular Length from the DFT-Optimized Junctions $L = d_{r\cdots r}$ (nm), Where r = N or S Atoms, Bond Length between the Top Gold Atoms of Gold Electrodes and the Anchor Atoms in the Relaxed Junctions, X (nm)

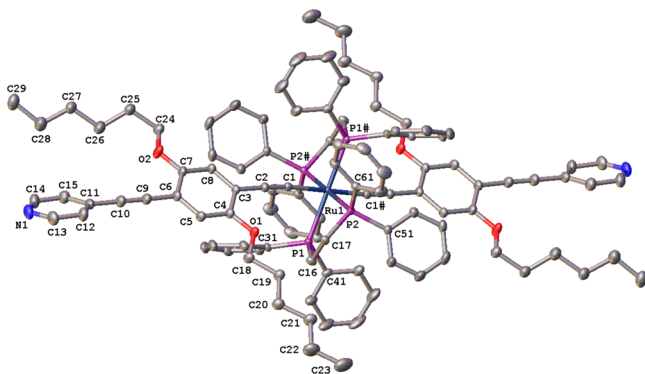| molecule	E_{HOMO} (eV)	E_{LUMO} (eV)	exp G/G_0	th G/G_0	Z^* (nm)	L (nm)	X (nm)	contacting group (Y)
1-Ru	−4.42	−1.46	4.5×10^{-6}	5.4×10^{-6}	3.1	2.9	0.23	$4\text{-}C_5H_4N$
1-Pt	−4.69	−1.48	9.8×10^{-6}	8.7×10^{-6}	3.0	2.86	0.23	$4\text{-}C_5H_4N$
2-Ru	−4.18	−1.07	1.8×10^{-5}	1.8×10^{-5}	2.4	2.65	0.245	$4\text{-}C_6H_4SMe$
2-Pt	−4.40	−1.12	1.8×10^{-5}	1.78×10^{-5}	2.5	2.68	0.245	$4\text{-}C_6H_4SMe$

Figure 1. Plot of the molecule **1-Ru** with thermal ellipsoids at 50% probability. Solvent molecules and hydrogen atoms have been omitted for clarity. Torsion angle C(7)−C(6)−C(11)−C(12): 145.4(2)°. N(1)−N(1′): 28.624(3) Å.
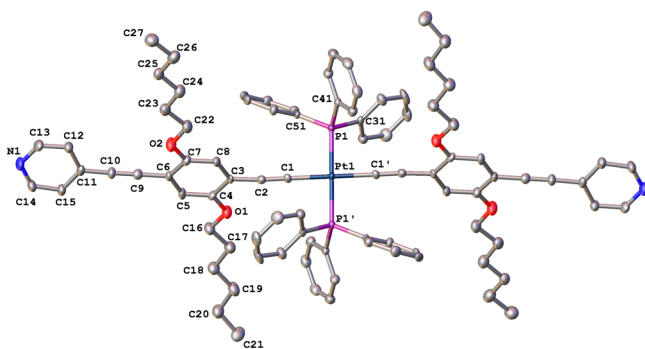
Figure 2. Plot of the molecule **1-Pt** with the thermal ellipsoids at 50% probability. Solvent molecules and hydrogen atoms have been omitted for clarity. Torsion angle C7−C6−C11−C15: 164.6(2)°. N(1)−N(1′): 28.620(7) Å.
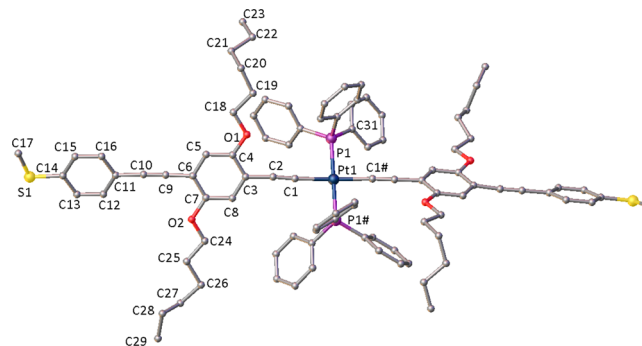

Figure 3. Plot of the molecule **2-Pt**. Solvent molecules and hydrogen atoms have been omitted, and only one component of a disordered hexyloxy side chain is shown for clarity. Torsion angle C7−C6−C11−C16: 165(1)°. S(1)−S(1′): 31.83(2) Å.

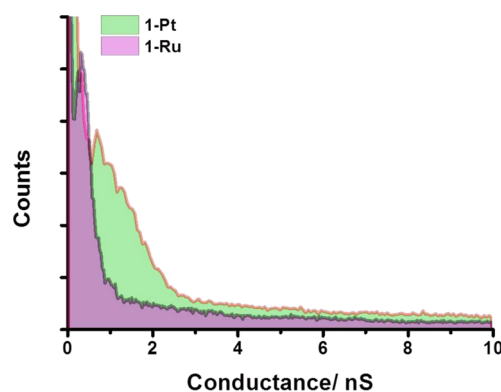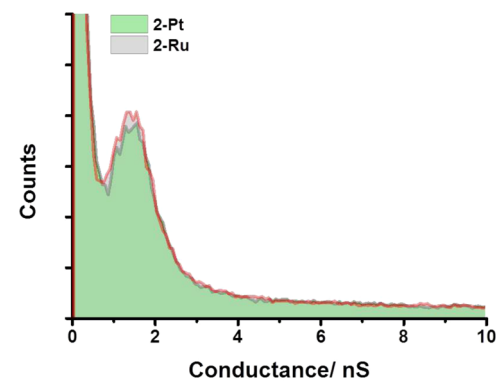**Figure 4.** $I(s)$ conductance histograms of **1-Ru** and **1-Pt** constructed from 500 traces.

Figure 5. $I(s)$ conductance histograms of **2-Ru** and **2-Pt** constructed from 500 traces.

sample (Figure 3), which is consistent with a rather more tilted arrangement of the molecule in the junction as might be expected from the geometry of the sulfur lone pairs in the thioether;[49] this interpretation has been supported by studies of the DFT-optimized junctions described in more detail below.

The conductance histograms constructed from 500 molecular junction formation traces with characteristic plateaus are shown in Figures 4 and 5. The peak conductance values from these histograms together with key data are summarized in Table 1. These conductance histograms reveal pronounced conductance peaks at 0.4 ± 0.18 nS (**1-Ru**), 0.8 ± 0.5 nS (**1-Pt**), 1.4 ± 0.4 nS (**2-Ru**), and 1.8 ± 0.6 nS (**2-Pt**), and within each pair of compounds featuring the same contacting group these values are indistinguishable. The 2−4-fold increase in conductance values of **2-Ru** and **2-Pt** in comparison with **1-Ru** and **1-Pt** further indicates the important role of the contacting group in the electrical response of the junction. However, in

contrast to the thiolate-contacted molecules derived from *trans*-$Ru(C{\equiv}CC_6H_4SAc)_2(dppm)_2$ (STM-BJ)[34] and *trans*-

HOMO   LUMO
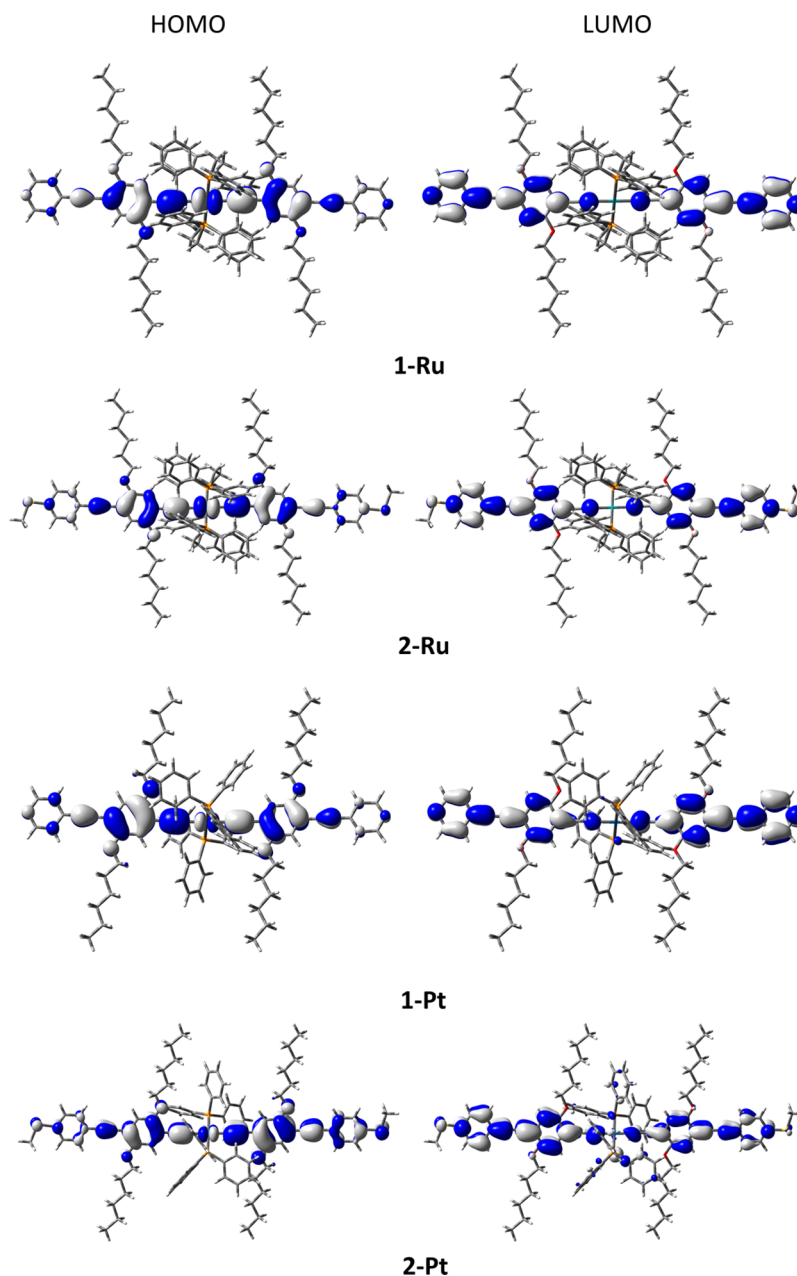

1-Ru

2-Ru

1-Pt

2-Pt

Figure 6. Plots of the HOMO and LUMO of **1-Ru**, **1-Pt**, **2-Ru**, and **2-Pt** (isosurfaces ± 0.02 (e/bohr^3)$^{1/2}$).

Pt(C≡CC$_6$H$_4$SAc)$_2$(PPh$_3$)$_2$ (MCBJ),[22] the differences in conductance as a function of the metallic moiety are negligible, and the platinum complexes are as conductive (or resistive) as the ruthenium analogues. The values for **1-Ru** and **1-Pt**, while low, are at least 1 order of magnitude higher than that of the "five-ring" organic compound NH$_4$C$_5$C≡C(C$_6$H$_2$R$_2$C≡C)$_3$C$_5$H$_4$N (R = OC$_6$H$_{13}$; $10^{-6.7}G_0$, 0.015 nS) of comparable molecular length (3 nm) (MCBJ data).[35]

In the quest to better understand these trends in conductance behavior, the electronic properties of the molecules and the electrical behavior of the junctions have been investigated by using DFT-based methods. Initial studies of the electronic structures of **1-Ru**, **1-Pt**, **2-Ru**, and **2-Pt** were carried out at the B3LYP level of theory[50] with a split LANL2DZ (Ru, Pt)/6-31G** (all other atoms) basis set.[51,52] Plots of the highest occupied and lowest unoccupied molecular orbitals (HOMO and LUMO, respectively) are given in Figure

6, and an analysis of the energy and distribution of the frontier molecular orbitals is summarized in Tables 1 and 2.

The HOMOs of the ruthenium complexes display the familiar pattern of dπ−pπ interactions along the metal−ethynyl axis[53] and extend along the molecular backbone. The nodal pattern of the HOMOs in the Pt complexes is similar, with a smaller metal contribution (Figure 6). The LUMOs are also delocalized over the molecular backbones and can largely be described as the π* system of the diethynylarylene ligands with little (Pt) or no (Ru) metal character. These varying metal contributions are reflected in the relative orbital energies, with the significant Ru contribution to the HOMO in **1-Ru** and **2-Ru** resulting in these orbitals lying some ca. 0.25 eV higher in energy than in the Pt analogues **1-Pt** and **2-Pt**. The largely organic π*-based LUMOs lead to less significant differences in LUMO energies, which differ by only 0.02−0.05 eV (Table 1).

Table 2. Composition (%) of the HOMO and LUMO of 1-Ru, 1-Pt, 2-Ru, and 2-Pt

	1-Ru		
	Ru	dppe	C≡CC$_6$H$_4$(OC$_6$H$_{13}$)$_2$C≡CC$_5$H$_4$N
LUMO	0	2	98
HOMO	25	3	72
	1-Pt		
	Pt	PPh$_3$	C≡CC$_6$H$_4$(OC$_6$H$_{13}$)$_2$C≡CC$_5$H$_4$N
LUMO	2	3	95
HOMO	6	2	92
	2-Ru		
	Ru	dppe	C≡CC$_6$H$_4$(OC$_6$H$_{13}$)$_2$C≡CC$_6$H$_4$SMe
LUMO	0	2	97
HOMO	22	3	76
	2-Pt		
	Pt	PPh$_3$	C≡CC$_6$H$_4$(OC$_6$H$_{13}$)$_2$C≡CC$_6$H$_4$SMe
LUMO	4	10	86
HOMO	5	1	94

However, these frontier orbital distributions per se do not provide evidence relating to the mechanisms of conductance, which is instead dominated by the alignment of the key molecular orbitals with the Fermi level of the electrodes. As noted by Georgiev and McGrady in computational studies of the conductance properties of extended metal atom chain complexes, the dominant conductance channel need not necessarily be associated with a molecular orbital evenly distributed along the molecular backbone; for example, a dominant conduction channel in Cr$_3$(dpa)$_4$(NCS)$_2$ (dpa = dipyridylamide) is derived from a nonbonding combination of metal d$_{z^2}$ orbitals directed along the Cr−Cr−Cr axis and localized on the terminal chromium atoms.[54]

To provide further insight into the experimentally observed trends obtained using the $I(s)$ technique, and to better evaluate the properties and behavior of these molecular junctions, calculations using a combination of DFT and a nonequilibrium Green's function formalism were also carried out. For the transport calculations, eight layers of (111)-oriented bulk gold with each layer consisting of 6 × 6 atoms and a layer spacing of 0.235 nm were used to create the molecular junctions, as shown in Figure 7 and described in detail elsewhere.[55] These layers were then further repeated to yield infinitely long current-carrying gold electrodes. Each molecule was attached to two (111)-directed gold electrodes; one of these electrodes was pyramidal, representing the STM tip, while the other was a planar slab representing the electrode formed by the idealized Au(111) substrate in the $I(s)$-based molecular junction. The molecules and first layers of gold atoms within each electrode were then allowed to relax again, to yield the optimal junction geometries shown in Figure 7. From these model junctions the transmission coefficient, $T(E)$, was calculated using the GOLLUM code.[55]

It is well-known that the Fermi energy predicted by DFT is often not reliable, and as such the room-temperature electrical conductance G was computed for a range of Fermi energies E_F; the calculated G is plotted as a function of $E_F − E_F^{DFT}$ in Figure 8. This multipoint fitting of the Fermi energy is a commonly accepted procedure in DFT-based calculations in molecular electronics.[56] To determine E_F, the predicted conductance values of all molecules were compared with the experimental values and a single common value of E_F was chosen, which gave
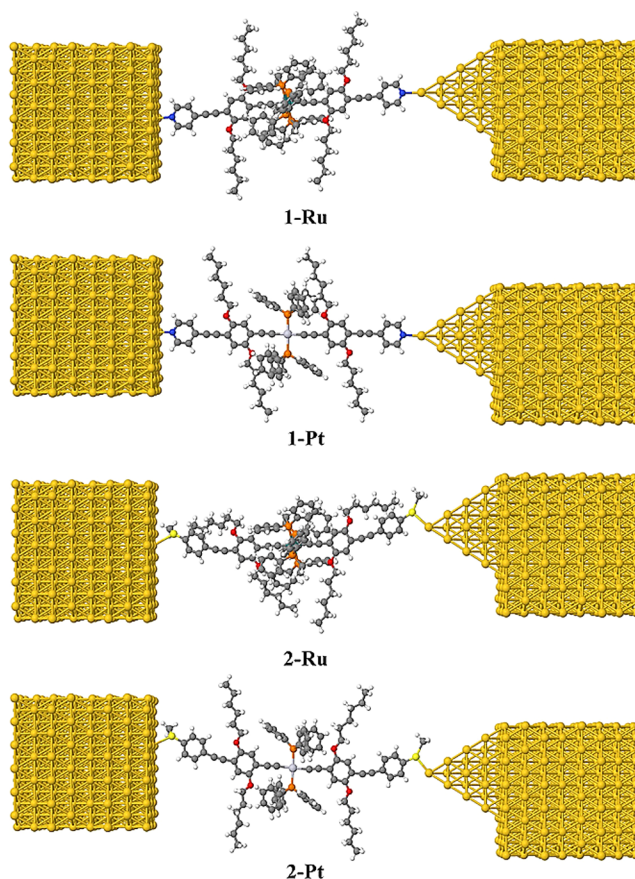
Figure 7. Relaxed geometries of molecular junctions of **1-Ru**, **1-Pt**, **2-Ru**, and **2-Pt**.
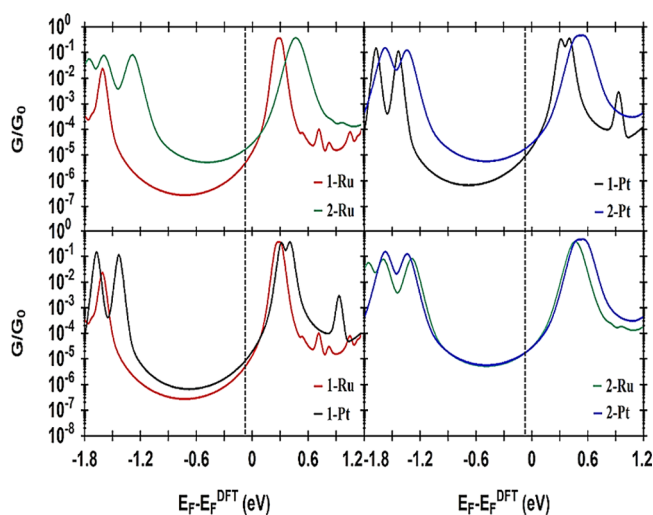
Figure 8. Plots showing selected comparisons of calculated conductance as a function of the Fermi energy for molecular junctions **1-Ru**, **1-Pt**, **2-Ru**, and **2-Pt**. Black dashed lines show the chosen Fermi energy ($E_F = −0.07$ eV).

the closest overall agreement. This yielded a surprisingly small value of $E_F − E_F^{DFT} = −0.07$ eV, which has been used in all of the theoretical results described below. Thygesen and colleagues have discussed similar situations for C$_{60}$-contacted molecular wires and shown that critical molecular orbitals can become pinned close to the Fermi level due to partial charge transfer and leading to good quantitative agreement between

calculated and experimentally determined conductance.[57] As shown below, the LUMO states of **1-M** and **2-M** (**M** = Ru, Pt) tail near the Fermi level in a manner similar to that in the Thygesen system, and partial charge transfer may also be responsible for the good agreement observed here.

The optimized junction geometries conform well to a description of the pyridine contacted compounds **1-Ru** and **1-Pt** forming point contacts between the pyridine nitrogen atom and the undercoordinated gold atoms of the gold electrodes. As expected, Figure 7 shows that the methyl thioether contacted compounds **2-Ru** and **2-Pt** are not oriented normal to the idealized, flat electrode surface within the molecular junction. Rather, they are tilted within molecular junctions to accommodate the directionality of the lone pairs of electrons on the sulfur atoms that bind to the gold electrodes.[49,58] The calculated molecular lengths and experimental break-off distances are consistent with these interpretations (Table 1).

The results of the room-temperature conductance calculations are summarized in Table 1, and comparisons between pairs of molecules according to contacting group and metal complex fragment are illustrated in Figure 8. It is immediately apparent that the conductance of the methyl thioether contacted molecules **2-M** is approximately 3−4 times higher than that of the analogous pyridine contacted species **1-M**, in good agreement with the experimental trends (Figure 8, top row, and Table 1). The greater conductance of the methyl thioether contacted compounds **2-M** likely arises from the greater Au−S bond strength and the broadening of the LUMO resonances arising from these interactions versus the pyridine-contacted analogues **1-M**.

More surprising is the limited influence of the metal−phosphine fragment on the molecular conductance (Figure 8, bottom row), which can be explained by the relative energy of the Fermi level and the molecular LUMOs together with a conductance mechanism based on a tunneling process through the tails of the respective LUMO states. Although tunneling through pyridine terminated compounds is usually attributed to LUMO-based transport,[43,59,60] the methyl thioether contact has been shown to permit both HOMO- and LUMO-based conductance mechanisms, depending on the nature of the molecular backbone.[61] Here it appears that the similar conductance values obtained from both series of compounds reflect the similar natures, energies, and compositions of the LUMOs, which provide a conductance channel between the electrodes. This contrasts with the recently reported single-molecule conductance studies of $trans$-Ru(C≡CC$_5$H$_4$N)(LL)$_2$ (LL = dppe, dmpe, {P(OMe)$_3$}$_2$) with the shorter alkynylpyridine ligands, in which the ligand π^* levels are likely to be much higher in energy than the extended alkynyl-based ligands in compounds **1-M** and **2-M**, and a HOMO-mediated conductance channel is proposed.[28]

In summary, the single-molecule conductance of two pairs of $trans$-bis(alkynyl) organometallic complexes based on Ru(dppe)$_2$ and Pt(PPh$_3$)$_2$ fragments and methyl thioether and pyridyl surface contacting groups have been studied in molecular junctions formed by the $I(s)$ method. Perhaps surprisingly, the nature of the metal moiety is a less significant point of chemical control over the electrical properties of the junction, with Pt(PPh$_3$)$_2$-based complexes being essentially as conductive (or as resistive) as the analogous Ru(dppe)$_2$ derivatives. The conductance of these compounds is more dependent on the position of the LUMO resonance with respect to the Fermi level of the junction and is largely influenced by the electrode−molecule contact. The energies and distributions of the molecular LUMOs are qualitatively similar in all of the compounds studied here and can be well described as the ethynylarylene ligand π^* orbitals. Given the rather straightforward synthetic chemistry associated with the preparation of long-chain ethynylarylene ligands, this work opens new avenues for the design of metal complex based molecular wires, including those based on readily available $trans$-bis(alkynyl) Pt(II) complexes.

■ EXPERIMENTAL SECTION

General Conditions. All reactions were carried out in oven-dried glassware under an oxygen-free argon atmosphere using standard Schlenk techniques. Diisopropylamine and triethylamine were purified by distillation from KOH; other reaction solvents were purified and dried using an Innovative Technology SPS-400 system and degassed before use. The compounds [RuCl(dppe)$_2$]OTf,[62] cis-PtCl$_2$(PPh$_3$)$_2$,[63] and 1,4-bis(hexyloxy)-2,5-diiodobenzene[64] were prepared by literature methods. Other reagents and intermediates were prepared by variations on literature methods as described below or purchased commercially and used as received.

NMR spectra were recorded in deuterated solvent solutions on Bruker Avance 400 MHz and Varian VNMRS 700 MHz spectrometers and referenced against residual protio solvent resonances (CHCl$_3$, ^{1}H 7.26 ppm and ^{13}C 77.00 ppm; CH$_2$Cl$_2$, ^{1}H 5.32 ppm and ^{13}C 53.84 ppm). In the NMR assignment, the phenyl ring associated with the dppe and PPh$_3$ is denoted Ph. Ar indicates any arylene group belonging to the alkynyl ligands.

Matrix-assisted laser desorption ionization (MALDI) mass spectra were recorded an using Autoflex II TOF/TOF mass spectrometer with a 337 nm laser. Infrared spectra were recorded on a Thermo 6700 spectrometer from CH$_2$Cl$_2$ solution in a cell fitted with CaF$_2$ windows.

2-Iodo-5-((trimethylsilyl)ethynyl)-1,4-bis(hexyloxy)-benzene.[64] In a 250 mL Schlenk flask, a solution of 1,4-bis(hexyloxy)-2,5-diiodobenzene (6.0 g, 11 mmol), (trimethylsilyl)-acetylene (490 mg, 0.7 mL, 5 mmol), PdCl$_2$(PPh$_3$)$_2$ (140 mg, 0.2 mmol), and CuI (38 mg, 0.2 mmol) in degassed dry Et$_3$N (120 mL) was stirred overnight at room temperature. The solvent was removed and the residue purified on a silica column. Elution with hexane allowed recovery of unreacted 1,4-bis(hexyloxy)-2,5-diiodobenzene, followed by elution with CH$_2$Cl$_2$/hexane (1/9), which after evaporation of the solvent produced a yellowish oil of the desired monoalkyne. Yield: 1.88 g (76%). ^{1}H NMR (400 MHz, CDCl$_3$): δ 7.25 (s, 1H, Ar); 6.83 (s, 1H, Ar); 3.95−3.92 (td, (J = 6.4, 1.4 Hz, 4H, −OCH$_2$); 1.81−1.76 (m, 4H, CH_2); 1.52−1.48 (m, 4H, CH_2); 1.36−1.33 (m, 8H, CH_2); 0.93−0.88 (m, 6H, CH$_2$CH_3); 0.25 (s, 9H, SiMe$_3$) ppm.

2-((Triisopropylsilyl)ethynyl)-5-((trimethylsilyl)ethynyl)-1,4-bis(hexyloxy)benzene.[22] To a solution of 2-iodo-5-((trimethylsilyl)ethynyl-1,4-bis(hexyloxy)benzene (1.88 g, 3.8 mmol) in degassed Et$_3$N (30 mL) were added (triisopropylsilyl)acetylene (TIPSA; 638 mg, 0.78 mL, 3.5 mmol), Pd(PPh$_3$)$_4$ (219 mg, 0.19 mmol), and CuI (36 mg, 0.19 mmol). The reaction mixture was stirred overnight at room temperature. The solvent was removed, and the residue was purified by passage through a silica pad and elution by ethyl acetate EtOAc/hexane (1/9) to give a yellow oil, which solidified to give an off-white solid on standing. Yield: 1.30 g (60%). ^{1}H NMR (400 MHz, CDCl$_3$): δ 6.88 (s, 1H, Ar); 6.87 (s, 1H, Ar); 3.97−3.91 (dt, J = 12.7, 6.4 Hz, 4H, −OCH$_2$); 1.82−1.72 (m, 4H, CH_2); 1.53−1.43 (m, 4H, CH_2); 1.35−1.30 (m, 8H, CH_2); 1.13 (s, 21H, SiPr^i_3); 0.92−0.88 (m, 6H, CH$_2$CH_3); 0.25 (s, 9H, SiMe_3) ppm.

2-((Triisopropylsilyl)ethynyl)-5-ethynyl-1,4-bis(hexyloxy)-benzene (1).[22] Potassium caronate (298 mg, 2.16 mmol) was added to a solution of 2-((triisopropylsilyl)ethynyl)-5-((trimethylsilyl)-ethynyl)-1,4-bis(hexyloxy)benzene (1.20 g, 2.16 mmol) in THF/MeOH (1/1) (160 mL). The solution was stirred for 2 h before CH$_2$Cl$_2$ was added. The solution was washed with water and the organic layer was collected and dried over MgSO$_4$, before the solvent was removed to yield an orange solid, which was used without further

purification. Yield: 950 mg (91%). ^{1}H NMR (700 MHz, CDCl$_3$): δ 6.91, 6.89 (2s, 2 × 1H, Ar); 3.98 (t, J = 6.5 Hz, 2H, −OCH$_2$); 3.92 (t, J = 6.5 Hz, 2H, −OCH$_2$); 3.31 (s, 1H, C≡CH); 1.83−1.72 (m, 4H, CH$_2$); 1.49−1.44 (m, 4H, CH$_2$); 1.35−1.30 (m, 8H, CH$_2$); 1.13 (s, 21H, SiPr$^i_3$); 0.92−0.87 (m, 6H, CH$_2$CH$_3$) ppm. ^{13}C{^{1}H} NMR (101 MHz, CDCl$_3$): δ 154.1 (O-C_{Ar}); 153.9 (O-C_{Ar}); 117.6, 117.2 (HC$_{Ar}$); 114.6, 112.6 (C_{Ar}); 102.7, 96.6 (C≡); 82.1 (H-C≡); 80.1 (C≡); 69.7, 69.3 (O-CH$_2$); 31.7, 31.5, 29.4, 29.1, 25.8, 25.6, 22.62, 22.57 (CH$_2$); 18.7 (H$_3C_{SiPr3}$); 14.1, 14.0 (CH$_3$); 11.4 (HC$_{SiPr3}$) ppm.

trans-Ru[C≡C{1,4-C$_6$H$_2$(OC$_6$H$_{13}$)$_2$}C≡CSiPr$^i_3$]$_2$(dppe)$_2$ (2). The complex salt [RuCl(dppe)$_2$]OTf (100 mg, 0.09 mmol) was added to a degassed solution of CH$_2$Cl$_2$ (4 mL) containing 1,8-diazabicyclo[5.4.0]undec-7-ene (DBU; 4 drops). The solution changed from red to orange with the addition of **1** (96 mg, 0.20 mmol). The reaction mixture was stirred for 1 h at room temperature before TlBF$_4$ (27 mg, 0.09 mmol) was added. After 20 min, the resulting solution had turned yellow and formed a precipitate (TlCl). The precipitate was removed by filtration through a Millex syringe filter (Millipore) to give an orange solution, which was reduced to the minimum volume, whereupon methanol (5 mL) was added. A yellow precipitate was obtained upon further concentration of the mixture. The product was collected by filtration and dried in air to give **2** as a bright yellow solid. Yield: 131 mg (76%). ^{1}H NMR (400 MHz, CDCl$_3$): δ 7.44 (m, 16H, Ph$_o$); 7.08−7.04 (m, 8H, Ph$_p$); 6.86−6.82 (m, 18H, (16H, Ph$_m$ + 2H, Ar); 5.86 (s, 2H, Ar); 3.84 (t, J = 6.9 Hz, 4H, O−CH$_2$); 3.64 (t, J = 6.4 Hz, 4H, O−CH$_2$); 2.89 (m, 8H, PCH$_2$CH$_2$P); 1.73−1.61 (m, 8H, CH$_2$); 1.48−1.46 (m, 4H, CH$_2$); 1.34−1.30 (m, 12H, CH$_2$); 1.18 (bs, 50H, (42H, SiPr$^i_3$ + 8H, CH$_2$); 0.92 (t, J = 7.0 Hz, 6H, CH$_2$CH$_3$); 0.81 (t, J = 7.0 Hz, 6H, CH$_2$CH$_3$) ppm. ^{31}P{^{1}H} NMR (162 MHz, CDCl$_3$): δ 52.07 (s) ppm. ^{13}C{^{1}H} NMR (101 MHz, CDCl$_3$): δ 154.3, 152.6 (−OCH$_{Ar}$); 137.3 (t, J = 11.4 Hz, Ph$_i$); 134.1 (Ph); 128.3 (Ph); 126.8 (Ph); 121.8 (C≡ or C_{Ar}); 117.2, 115.2 (HC$_{Ar}$); 114.7, 106.5, 104.9, 93.2 (C≡ or C_{Ar}); 68.9 (−OCH$_2$); 68.7 (−OCH$_2$); 31.74 (P-CH$_2$) overlapping with CH$_2$; 31.69, 29.6, 27.5, 25.9, 25.8, 22.7, 22.6 (CH$_2$); 18.8 (H$_3C_{SiPr3}$); 14.1 (CH$_3$); 14.0 (CH$_3$); 11.5 (HC$_{SiPr3}$) ppm. IR (CH$_2$Cl$_2$): ν(C≡CSiPr$^i_3$) 2138 (m); ν(RuC≡C) 2050 (s) cm^{-1}. MS$^+$ (MALDI-TOF; m/z): 898.1 [Ru(dppe)$_2$]$^+$; 1861.9 [M]$^+$. HR-ESI$^+$-MS: m/z calcd for C$_{114}$H$_{146}$O$_4$P$_4$^{96}RuSi$_2$ 1856.8895; found 1856.8856.

trans-Ru[C≡C-{1,4-C$_6$H$_2$(OC$_6$H$_{13}$)$_2$}C≡CH]$_2$(dppe)$_2$ (3). Tetra-n-butylammonium fluoride (TBAF; 1.0 M in tetrahydrofuran; 0.24 mL, 0.24 mmol) was added to a solution of **2** (180 mg, 0.1 mmol) in THF (15 mL). The solution was stirred overnight at room temperature. The resulting mixture was dried and purified on neutral alumina with CH$_2$Cl$_2$/hexane (50/45) as eluent with 5% Et$_3$N to give a yellow solid (100 mg, 0.06 mmol, 60%). Crystals suitable for X-ray diffraction were grown by slow diffusion of MeOH into a CH$_2$Cl$_2$ solution of **3** containing 5% Et$_3$N. ^{1}H NMR (400 MHz, CDCl$_3$): δ 7.45−7.43 (m, 16H, Ph$_o$); 7.09−7.05 (m, 8H, Ph$_p$); 6.89 (s, 2H, Ar); 6.87−6.83 (m, 16H, Ph$_m$); 5.83 (s, 2H, Ar); 3.86 (t, J = 7.0 Hz, 4H, O−CH$_2$); 3.67 (t, J = 7.0 Hz, 4H, O-CH$_2$); 3.31 (s, 2H, C≡CH); 2.93−2.89 (m, 8H, PCH$_2$CH$_2$P); 1.75−1.64 (m, 8H, CH$_2$); 1.43−1.41 (m, 4H, CH$_2$); 1.36−1.30 (m, 12H, CH$_2$); 1.23−1.20 (m, 8H, CH$_2$); 0.92 (t, J = 7.0 Hz, 6H, CH$_2$CH$_3$); 0.82 (t, J = 7.0 Hz, 6H, CH$_2$CH$_3$) ppm. ^{31}P NMR {^{1}H} NMR (162 MHz, CDCl$_3$): δ 51.85 (s) ppm. ^{13}C{^{1}H} NMR (101 MHz, CDCl$_3$): δ 154.0, 152.6 (−OCH$_{Ar}$); 137.2 (t, J = 15.5 Hz, Ph$_i$); 134.1 (Ph); 128.4 (Ph); 126.9 (Ph); 122.3 (C≡ or C_{Ar}); 117.7, 115.3 (HC$_{Ar}$); 114.5, 104.9 (C≡ or C_{Ar}); 81.7 (H-C≡); 80.0 (C≡); 69.0 (−OCH$_2$); 68.9 (−OCH$_2$); 31.6 (P-CH$_2$) overlapping with CH$_2$; 31.5, 30.1, 29.5, 29.3, 25.8, 25.6, 22.64, 22.58 (CH$_2$); 14.05 (CH$_3$); 14.02 (CH$_3$) ppm (one quaternary ^{13}C≡ was not detected). MS$^+$(MALDI-TOF; m/z): 898.0 [Ru(dppe)$_2$], 1548.4 [M]$^+$. IR (CH$_2$Cl$_2$): ν(≡CH) 3301 (m); ν(RuC≡C) 2049 (s) cm^{-1}. HR-ESI$^+$-MS: m/z calcd for C$_{96}$H$_{106}$O$_4$P$_4$Ru 1548.6113; found 1548.6082.

trans-Ru[C≡C-{1,4-C$_6$H$_2$(OC$_6$H$_{13}$)$_2$}C≡CC$_5$H$_4$N]$_2$(dppe)$_2$ (1-Ru). Compound **3** (120 mg, 0.077 mmol), 4-iodopyridine (39 mg, 0.192 mmol), Pd(PPh$_3$)$_4$ (4.6 mg, 0.004 mmol), and CuI (0.8 mg, 0.004 mmol) were added to a degassed solution of NH^{i}Pr$_2$ (10 mL). The yellow solution was heated at 80 °C for 20 h, during which time

the solution turned orange with a precipitate developing. The precipitate was removed by filtration, and the solid was washed with methanol to remove ammonium salts, giving a yellow powder. Yield: 85 mg (64%). Crystals suitable for X-ray diffraction were grown by slow diffusion of MeOH into a CH$_2$Cl$_2$ solution of **1-Ru** containing 5% Et$_3$N. ^{1}H NMR (400 MHz, CD$_2$Cl$_2$): δ 8.57 (d, J = 5.2 Hz, 4H, C$_6$H$_4$N); 7.52−7.40 (m, 16H, Ph$_o$); 7.37 (d, J = 5.2 Hz, 4H, C$_6$H$_4$N); 7.13−7.11 (m, 8H, Ph$_p$); 6.95 (s, 2H, Ar); 6.90−6.87 (m, 16H, Ph$_m$); 5.84 (s, 2H, Ar); 3.93 (t, J = 6.5 Hz, 4H, −OCH$_2$); 3.68 (t, J = 7.2 Hz, 4H, O-CH$_2$); 2.96−2.93 (m, 8H, PCH$_2$CH$_2$P); 1.79−1.74 (m, 8H, CH$_2$); 1.52−1.50 (m, 4H, CH$_2$); 1.38−1.36 (m, 12H, CH$_2$); 1.26−1.23 (m, 8H, CH$_2$); 0.94−0.92 (pseudo-t, 6H, CH$_2$CH$_3$); 0.84−0.82 (pseudo-t, 6H, CH$_2$CH$_3$) ppm. ^{31}P{^{1}H} NMR (162 MHz, CD$_2$Cl$_2$): δ 51.7 (s) ppm. ^{13}C{^{1}H} NMR (101 MHz, CD$_2$Cl$_2$): δ 154.3, 153.3 (-OC$_{Ar}$); 150.1 (HC$_{C5H4N}$); 137.7 (t, J = 10.9 Hz, Ph$_i$); 134.5 (Ph); 132.6 (C_{C5H4N}); 128.9 (Ph); 127.3 (Ph); 125.4 (HC$_{C5H4N}$); 123.3 (C≡ or C_{Ar}); 117.9, 114.9 (HC$_{Ar}$); 105.3 (C≡ or C_{Ar}); 93.2, 90.7 (C≡); 69.4, 69.3 (O-CH$_2$); 32.1 (P-CH$_2$); 32.0, 29.5, 29.4, 25.8, 22.7, 22.6 (CH$_2$); 13.9 (CH$_3$); 13.8 (CH$_3$) the other quaternary ^{13}C≡ were not detected. IR (CH$_2$Cl$_2$): ν(C≡CC$_5$H$_4$N) 2208 (m); ν(RuC≡C) 2044 (s) cm^{-1}. MS$^+$ (MALDI-TOF; m/z): 898.0, [Ru(dppe)$_2$]$^+$; 1702.6, [M]$^+$. HR-ESI$^+$-MS: m/z calcd for C$_{106}$H$_{112}$N$_2$O$_4$P$_4$^{96}Ru 1697.6682; found 1697.6688. Anal. Calcd for C$_{106}$H$_{112}$N$_2$O$_4$P$_4$Ru: C, 74.76; H, 6.63; N, 1.64. Found: C, 74.66; H, 6.72; N, 1.70. Crystal data for **1-Ru**: C$_{106}$H$_{112}$N$_2$O$_4$P$_4$Ru, M_r = 1524.70, triclinic, space group $P\bar{1}$, a = 12.3676(7) Å, b = 12.9676(7) Å, c = 13.9333(8) Å, α = 83.888(2)°, β = 83.489(2)°, γ = 80.585(2)°, U = 2181.4(2) Å^3, F(000) = 898.0, Z = 1, D_c = 1.296 mg m^{-3}, μ = 0.309 mm^{-1}; 47816 reflections collected yielding 12134 unique data (R_{int} = 0.0244). Final wR2(F^2) = 0.0952 for all data (531 refined parameters), conventional R1(F) = 0.0356 for 11015 reflections with $I \geq 2\sigma$, GOF = 1.065.

trans-Pt[C≡C{1,4-C$_6$H$_2$(OC$_6$H$_{13}$)$_2$}C≡CSiPr$^i_3$]$_2$(PPh$_3$)$_2$ (5). A mixture of **1** (250 mg, 0.52 mmol) and CuI (4 mg) was added to a solution of _cis_-PtCl$_2$(PPh$_3$)$_2$ (200 mg, 0.26 mmol) in dry and degassed diethylamine (NHEt$_2$; 20 mL). The orange reaction mixture was heated to 100 °C for 2 h. The solvent was removed, and the remaining residue was purified on a silica column with CH$_2$Cl$_2$ as eluent. The resulting product was obtained as an amorphous orange solid. Yield: 320 mg (81%). ^{1}H NMR (400 MHz, CDCl$_3$): δ 7.82−7.77 (m, 12H, Ph); 7.31−7.24 (m, 18H, Ph); 6.63 (s, 2H, Ar); 5.71 (s, 2H, Ar); 3.60 (t, J = 6.5 Hz, 4H, O-CH$_2$); 3.49 (t, J = 6.8 Hz, 4H, O-CH$_2$); 1.71−1.63 (m, 4H, CH$_2$); 1.46−1.39 (m, 4H, CH$_2$); 1.32−1.27 (m, 24H, CH$_2$); 1.10 (s, 42H, SiPr$^i_3$); 0.91 (t, J = 7.0 Hz, 6H, CH$_2$CH$_3$); 0.86 (t, J = 7.0 Hz, 6H, CH$_2$CH$_3$) ppm. ^{31}P{^{1}H} NMR (162 MHz, CDCl$_3$): δ 17.43 (s, J_{P-Pt} = 2654.12 Hz) ppm. ^{13}C{^{1}H} NMR (101 MHz, CDCl$_3$): δ 154.1 (−OC$_{Ar}$); 152.2 (−OC$_{Ar}$); 135.3 (t, J = 6.0 Hz, Ph$_o$); 131.3 (t, J = 29.3 Hz, Ph$_i$); 130.1 (Ph$_p$); 127.6 (t, J = 5.4 Hz, Ph$_m$); 120.9 (C≡ or C_{Ar}); 118.9, 116.6 (HC$_{Ar}$); 109.1, 104.0, 93.8 (C≡ or C_{Ar}); 70.0, 68.9 (O-CH$_2$); 31.7, 31.6, 29.5, 29.2, 25.9, 25.5, 22.7, 22.6 (CH$_2$); 18.7 (H$_3C_{SiPr3}$); 14.1 (CH$_3$) (one visible); 11.4 (HC$_{SiPr3}$) ppm, the other quaternary ^{13}C≡ were not detected. IR (CH$_2$Cl$_2$): ν(C≡CSiPr$^i_3$) 2145 (m); ν(PtC≡C) 2103 (m) cm^{-1}. MS$^+$ (MALDI-TOF; m/z): 1682.5, [M]$^+$. HR-ESI$^+$-MS: m/z calcd for C$_{98}$H$_{128}$O$_4$P$_2$^{194}PtSi$_2$ 1682.8558; found 1682.8484.

trans-Pt[C≡C{1,4-C$_6$H$_2$(OC$_6$H$_{13}$)$_2$}C≡CH]$_2$(PPh$_3$)$_2$ (6). A solution of TBAF (1.0 M in THF; 0.38 mL, 0.38 mmol) was added to a solution of **5** (150 mg, 0.096 mmol) in THF (25 mL). The reaction mixture was stirred for 24 h at room temperature. The solvent was removed, the residue was redissolved in CH$_2$Cl$_2$, and this solution was washed with water, ammonium chloride (NH$_4$Cl, aqueous), and brine. The organic phase was dried (MgSO$_4$) and the solvent removed to give an amorphous yellow solid. The solid was purified on a short silica pad, with 5% NEt$_3$ in CH$_2$Cl$_2$ as eluent, and compound **6** was obtained by precipitation in CH$_2$Cl$_2$/MeOH. Yield: 130 mg (63%). ^{1}H NMR (400 MHz, CDCl$_3$): δ 7.83−7.78 (m, 12H, Ph); 7.32−7.25 (m, 18H, Ph); 6.65 (s, 2H, Ar); 5.74 (s, 2H, Ar); 3.64 (t, J = 7.0 Hz, 4H, O-CH$_2$); 3.48 (t, J = 7.0 Hz, 4H, O-CH$_2$); 3.19 (s, 2H, C≡CH); 1.73−1.66 (m, 4H, CH$_2$); 1.44−1.40 (m, 4H, CH$_2$); 1.34−1.13 (m, 24H, CH$_2$); 0.91 (t, J = 6.3 Hz, 6H, CH$_2$CH$_3$); 0.86 (t, J = 6.3 Hz, 6H, CH$_2$CH$_3$). ^{31}P{^{1}H} NMR (162 MHz, CDCl$_3$): δ 17.61 (s, J_{P-Pt} = 2648

Hz) ppm. $^{13}C\{^1H\}$ NMR (101 MHz, CDCl$_3$): δ 153.9, 152.3 ($-$OC$_{Ar}$); 135.2 (t, J = 6.2 Hz, Ph$_o$); 131.2 (t, J = 29.3 Hz, Ph$_i$); 130.1 (Ph$_p$); 127.6 (t, J = 5.4 Hz, Ph$_m$); 121.3 (C$_{Ar}$ or C≡); 119.4 (t, J = 15.1 Hz, C$_a$≡); 118.7, 116.9 (HC$_{Ar}$); 110.2, 107.6 (C$_{Ar}$ or C≡); 80.9 (H-C≡); 80.4 (C≡); 69.9, 69.2 (O-CH$_2$); 31.6, 29.2, 29.1, 25.6, 25.4, 22.61, 22.56 (CH$_2$); 14.1, 14.0 (CH$_3$) ppm. IR (CH$_2$Cl$_2$): ν(≡C$-$H) 3300 (w); ν(PtC≡C) 2098 (m) cm^{-1}. MS$^+$ (MALDI-TOF; m/z): 719.4 [Pt(PPh$_3$)$_2$]$^+$, 1371.1, [M]$^+$. HR-ESI$^+$-MS: m/z calcd for C$_{80}$H$_{88}$O$_4$P$_2$^{194}Pt 1369.5863; found 1369.5836.

***trans*-Pt[C≡C{1,4-C$_6$H$_2$(OC$_6$H$_{13}$)$_2$}C≡CC$_5$H$_4$N]$_2$(PPh$_3$)$_2$ (1-Pt).** Compound **6** (90 mg, 0.064 mmol), 4-iodopyridine (30 mg, 0.15 mmol), Pd(PPh$_3$)$_4$ (4 mg, 0.003 mmol), and CuI (0.8 mg, 0.004 mmol) were placed in a Schlenk flask charged with degassed Et$_3$N (10 mL), and the reaction mixture was heated for 2 h at 100 °C. The solvent was removed from the yellow solution and the residue purified by column chromatography on silica with CH$_2$Cl$_2$/hexane/Et$_3$N (8.5/1.5/0.5) as eluent to give a yellow solid. The solid was dissolved in the minimum amount of CH$_2$Cl$_2$, and MeOH (5 mL) was added. Concentration of the solution caused the desired **1-Pt** to precipitate. Yield: 30 mg (30%). Crystals suitable for X-ray diffraction were grown by slow diffusion of MeOH into a CH$_2$Cl$_2$ solution of **1-Pt** containing 5% NEt$_3$. ^{1}H NMR (400 MHz, CDCl$_3$): δ 8.54 (pseudo-d, 4H, C$_5$H$_4$N), 7.83$-$7.81 (m, 12H, Ph), 7.33$-$7.26 (m, 22H, (18H, Ph + 4H, C$_5$H$_4$N), 6.69 (s, 2H, Ar), 5.78 (s, 2H, Ar), 3.68 (pseudo-t, 4H, O-CH$_2$), 3.53 (pseudo-t, 4H, O-CH$_2$), 1.76$-$1.72 (m, 4H, CH$_2$), 1.50$-$1.47 (m, 4H, CH$_2$), 1.38$-$1.16 (m, 24H, CH$_2$), 0.92$-$0.85 (m, 12H, CH$_2$CH$_3$) ppm. ^{31}P{^{1}H} NMR (162 MHz, CDCl$_3$): δ 17.67 (s, J_{P-Pt} = 2643.5 Hz) ppm. ^{13}C{^{1}H} NMR (101 MHz, CDCl$_3$): δ 153.8, 152.5 ($-$OC$_{Ar}$), 149.5 (HC$_{C5H4N}$), 135.2 (t, J = 6.2 Hz)) (Ph$_o$), 131.2 (t, J = 29.1 Hz)) (Ph$_i$), 130.1 (Ph$_p$), 127.6 (t, J = 5.4 Hz)) (Ph), 125.3 (HC$_{C5H4N}$), 117.9, 116.9 (HC$_{Ar}$), 107.6 (C≡ or C$_{Ar}$), 92.0, 90.5, 69.9, 69.2 (C≡) other quaternary ^{13}C were not seen, 31.60, 31.57, 29.3, 29.1, 25.7, 25.4, 22.65, 22.56 (CH$_2$), 14.1, 14.0 (CH$_3$) ppm. IR (CH$_2$Cl$_2$): 2112 (m) ν(C≡CC$_5$H$_4$N) 2102 (s) ν(PtC≡C) cm^{-1}. MS$^+$ (MALDI-TOF; m/z): 1524.5 [M]$^+$. HR-ESI+-MS: m/z calcd for C$_{90}$H$_{95}$N$_2$O$_4$P$_2$^{194}Pt 1523.6394; found 1523.6362. Anal. Calcd for C$_{90}$H$_{94}$N$_2$O$_4$P$_2$Pt: C, 70.89; H, 6.21; N, 1.84. Found: C, 70.72; H, 6.13; N, 1.93. Crystal data for **1-Pt**: C$_{90}$H$_{94}$N$_2$O$_4$P$_2$Pt, M_r = 1702.93, triclinic, space group $P\bar{1}$, a = 9.5706(4) Å, b = 13.1673(6) Å, c = 16.6608(9) Å, α = 71.273(5)°, β = 86.786(4)°, γ = 71.249(4)°, U = 1880.3(2) Å^3, $F(000)$ = 788.0, Z = 1, D_c = 1.347 mg m^{-3}, μ = 1.962 mm^{-1}; 17913 reflections collected yielding 8632 unique data (R_{int} = 0.0719). Final wR2(F^2) = 0.1048 for all data (450 refined parameters), conventional R1(F) = 0.0535 for 7746 reflections with $I \geq 2\sigma$, GOF = 1.007.

***trans*-Ru[C≡C{1,4-C$_6$H$_2$(OC$_6$H$_{13}$)$_2$}C≡C(4-C$_5$H$_4$SMe)]$_2$(dppe)$_2$ (2-Ru).** Compound **3** (40 mg, 0.026 mmol), 4-iodothioanisole (13 mg, 0.052 mmol), Pd(PPh$_3$)$_4$ (1.5 mg, 0.001 mmol), and CuI (0.2 mg, 0.001 mmol) were added to a degassed solution of NH^{i}Pr$_2$ (5 mL). The yellow solution was heated at 80 °C for 24 h, and the precipitate was removed by filtration. The crude solid was purified on a neutral alumina column with CH$_2$Cl$_2$/5% NEt$_3$ as eluent to give a yellow powder after removing the solvent. Yield: 15 mg (34%). ^{1}H NMR (700 MHz, CD$_2$Cl$_2$): δ 7.45$-$7.43 (m, 20H, Ph (16H) + C$_6$H$_4$SMe (4H)), 7.23 (d, J = 7.8 Hz, 4H, C$_6$H$_4$SMe), 7.10 (t, J = 7.4 Hz, 8H, Ph), 6.92 (s, 2H, Ar), 6.88 (t, J = 7.6 Hz, 16H, Ph), 5.85 (s, 2H, Ar), 3.92 (t, J = 6.9 Hz, 4H, OCH$_2$), 3.68 (t, J = 6.4 Hz, 4H, OCH$_2$), 2.93 (s, 6H, C$_6$H$_4$S*Me*), 1.78$-$1.69 (m, 8H, CH$_2$), 1.38$-$1.35 (m, 12H, CH$_2$), 1.26$-$1.20 (m, 12H, CH$_2$), 0.96$-$0.89 (t, J = 6.6 Hz, 6H, CH$_2$CH$_3$), 0.82 (t, J = 6.9 Hz, 6H, CH$_3$). ^{31}P{^{1}H} NMR (162 MHz, CDCl$_3$): δ 51.8 (s) ppm. ^{13}C{^{1}H} NMR (700 MHz, CDCl$_3$): δ 153.9, 153.3 (O-CAr), 139.1, 137.8 (S-CAr), 134.5 (Ph), 131.8 (HCC$_6$H$_4$SMe), 128.9 (Ph), 127.3, 126.3 (Ph), 122.2, 120.9 (CAr), 118.1, 114.8 (HCAr), 106.7, 92.8, 88.2 (C≡), 69.41, 69.36 (OCH$_2$), 32.09, 32.07, 30.0, 29.9, 26.2, 23.1, 23.0 (CH$_2$), 15.7 (SCH$_3$), 14.3, 14.2 (CH$_3$). MS$^+$ (MALDI-TOF; m/z): 898.1 [Ru(dppe)$_2$]$^+$, 1793.3 [M + H]$^+$. IR (CH$_2$Cl$_2$): 2055s ν(Ru-C≡C) cm^{-1}. HR-ESI+-MS: calcd for C$_{110}$H$_{118}$O$_4$P$_4$RuS$_2$ 1792.6495; found 1792.6510.

***trans*-Pt[C≡C{1,4-C$_6$H$_2$(OC$_6$H$_{13}$)$_2$}C≡C(4-C$_5$H$_4$SMe)]$_2$(PPh$_3$)$_2$ (2-Pt).** Compound **6** (90 mg, 0.064 mmol), 4-iodothioanisole (37.5

mg, 0.15 mmol), Pd(PPh$_3$)$_4$ (4 mg, 0.003 mmol), and CuI (1 mg) were placed in a Schlenk flask charged with degassed HN^{i}Pr$_2$ (8 mL), and the reaction mixture was heated for 2 h at 100 °C. The yellow solution was evaporated to dryness, and the residue was purified on a silica column with CH$_2$Cl$_2$/hexane (1/1 v/v) followed by pure CH$_2$Cl$_2$ as eluent to give yellow crystals. Yield: 17 mg, 17%. X-ray-quality crystals were grown by slow diffusion of methanol into a solution of the complex in 95/5 CH$_2$Cl$_2$/NEt$_3$ (v/v). ^{1}H NMR (600 MHz, CDCl$_3$): δ 7.84$-$7.81 (m, 12H, Ph), 7.38 (d, J = 9.1 Hz, 4H, C$_6$H$_4$SMe), 7.33$-$7.27 (m, 18H, Ph), 7.17 (d, J = 9.1 Hz, 4H, C$_6$H$_4$SMe), 6.68 (s, 2H, Ar), 5.77 (s, 2H, Ar), 3.78 (t, J = 6.5 Hz, 4H, O-CH$_2$), 3.54 (t, J = 6.9 Hz, 4H, OCH$_2$), 2.48 (s, 6H, SCH$_3$), 1.76$-$1.71 (m, 4H, CH$_2$), 1.51$-$1.47 (m, 4H, CH2), 1.36$-$1.27 (m, 16H, CH2), 1.21$-$1.14 (m, 8H, CH$_2$), 0.91$-$0.86 (m, 12H, CH$_2$CH$_3$) ppm. ^{31}P{^{1}H} NMR (162 MHz, CDCl$_3$): δ 17.6 (s, J_{P-Pt} = 2653.1 Hz) ppm. ^{13}C{^{1}H} NMR (101 MHz, CDCl$_3$): δ 153.3, 152.5 (OCAr), 138.4 (S-CAr), 135.3 (t, J = 6.2 Hz, Ph), 131.6 (HCC$_6$H$_4$SMe), 131.3 (t, J = 29.2 Hz, Ph), 130.1 (Ph), 127.6 (t, J = 5.5 Hz, Ph), 125.9 (HCC$_6$H$_4$SMe), 120.7, 120.5 (CAr), 117.7, 117.2 (HCAr), 109.1, 92.9, 86.9 (C≡), 69.8, 69.2 (OCH$_2$), 31.64, 31.58, 29.4, 29.1, 25.8, 25.5, 22.7, 22.6 (CH$_2$), 15.5 (SCH$_3$), 14.12, 14.08 (CH$_3$) ppm. MS+ (MALDI-TOF; m/z): 719.4 [Pt(PPh$_3$)$_2$]$^+$, 1614.3 [M + H]$^+$. IR (CH$_2$Cl$_2$): ν(Pt-C≡C) 2104 (s) cm^{-1}. HR-(ESI+)-MS: calcd for C$_{94}$H$_{100}$O$_4$P$_2$PtS$_2$Na 1637.6107; found 1637.6124. Crystal data for **2-Pt**: C$_{94}$H$_{100}$O$_4$P$_2$PtS$_2$, M_r = 1614.89, monoclinic, space group $P2/n$, a = 22.659(10) Å, b = 9.469(4) Å, c = 22.765(10) Å, β = 118.005(5)°, U = 4313(3) Å^3, $F(000)$ = 1672.0, Z = 2, D_c = 1.622 mg m^{-3}, μ = 1.244 mm^{-1}, crystal size 0.01 × 0.01 × 0.001 mm^3; 42922 reflections collected yielding 8352 unique data (R_{int} = 0.2997). Final wR2(F^2) = 0.2517 for all data (371 refined parameters), conventional R1(F) = 0.0949 for 4614 reflections with $I \geq 2\sigma$, GOF = 1.024.

Single-Molecule Conductance Measurements. Gold-on-glass substrates (Arrandee, Schröer, Germany) were cleaned with acetone and flame-annealed with a butane torch until a slight orange hue was obtained. The slide was kept in this state for 20 s, during which time the torch was kept in motion around the sample to avoid overheating. This procedure was performed three times to generate flat Au (111) terraces.[65] The freshly annealed substrates were immersed in a 10^{-4} M mesitylene solution of the complex under investigation for 1 min, after which time the gold sample was removed and washed with ethanol and then dried under an argon flow. The short immersion time and low concentration of solution were chosen to promote low molecular coverage of the gold surface, which increases the formation of single-molecule events over aggregate phenomena.

Conductance values of the compounds and the break-off distances were obtained with an STM (Agilent 5500 SPM microscope), using the $I(s)$ technique, in which an electrochemically etched gold tip is approached close to the substrate surface and then retracted with the tunneling current (I) recorded against distance (s).[48] The Agilent 5500 SPM was fitted with a low-current preamplifier, and set point conditions of I = 30 nA and bias voltage U_{tip} = 0.6 V were employed. The $I(s)$ method involves repeatedly moving the STM tip toward the gold surface to given set-point values and then rapidly away from the surface. During these cycles molecular junctions are occasionally formed, which can be recognized by deviations from the usual exponential decay of current in the form of current plateaus. In this case as the junction is stretched beyond its maximum length, the molecular bridge breaks, leading to a sharp decrease in current and current steps. Hence, these junction formation and cleavage processes are recognized by plateaus and steps in the current-distance currents. Since the $I(s)$ technique is a "non-contact" method (no metallic contact between the gold STM tip and gold surface), the molecular junction formation probability, as recognized by the plateau-step traces, is significantly smaller than for break junction techniques. The $I(s)$ tip retraction cycles were repeated many times (normally 4000$-$5000 traces) in order to record sufficient traces where molecular junctions form, called molecular junction formation scans, as opposed to most traces for which no junction forms. Molecular junction formation scans are recognized by recording only traces which exhibit a plateau longer than 1 Å, present in about 15% of all traces for both

anchor groups. The resulting $I(s)$ curves are binned in current steps (16 pS) and plotted to give a conductance histogram comprised of at least 500 $I(s)$ scans showing plateaus. The error associated with each current value reported has been statistically obtained from the standard deviation of the points comprising the conductance peak.

Single-Crystal X-ray Crystallography. The X-ray single-crystal data for **1-Ru** have been collected using $\lambda(\text{Mo } K\alpha)$ radiation ($\lambda = 0.71073$ Å) on a Bruker D8Venture diffractometer (Photon100 CMOS detector, IμS-microsource, focusing mirrors) and for a crystal of **1-Pt** on an Agilent XCalibur diffractometer (Sapphire-3 CCD detector, fine-focus sealed tube, graphite monochromator) equipped with a Cryostream (Oxford Cryosystems) open-flow nitrogen cryostat at 120.0(2) K. The data for the extremely small and weakly diffracting crystal of **2-Pt** were collected at 100.0(2) K on a Rigaku Saturn 724+ diffractometer at station I19 of the Diamond Light Source (UK) synchrotron (undulator, $\lambda = 0.6889$ Å, ω scan, 1.0°/frame) and processed using Bruker APEXII software. All structures were solved by direct methods and refined by full-matrix least squares on F^2 for all data using Olex2[66] and SHELXTL[67] software. All nondisordered non-hydrogen atoms were refined anisotropically; the hydrogen atoms were placed in calculated positions and refined in riding mode. Disordered atoms in the structure of **2-Pt** were refined isotropically with fixed SOF = 0.6 and 0.4. The structure of **2-Pt** also contains severely disordered solvent molecules (probably DCM) which could not be reliably identified and modeled properly. Their contribution to the structural factors was taken into account by applying MASK procedure of Olex2 program package. Crystallographic data for the structures have been deposited with the Cambridge Crystallographic Data Centre as supplementary publications CCDC 1483157−1483159.

Theoretical Methods. Gas-phase optimizations were performed with the Gaussian 09 program package,[68] using the B3LYP functional[50] and LANL2DZ basis set on Ru and Pt[51] and 6-31G** on all other atoms.[52] Results were further analyzed using the GaussSum package.[69]

The DFT-Landauer approach used in the modeling of molecular junctions assumes that, on the time scale taken by an electron to traverse the molecule, inelastic scattering is negligible. This is known to be an accurate assumption for molecules up to several nanometers in length.[57] All molecules in this work have been relaxed in isolation. Geometry optimizations were carried out using the DFT code SIESTA, with a generalized gradient approximation (PBE functional),[70] double-ζ polarized basis set, 0.01 eV/A force tolerance, and a real-space grid with a plane wave cutoff energy of 250 Ry, zero bias voltage, and 1 k points.

To compute the electrical conductance, the molecules were then placed in the vicinity of the metal|molecule|metal junctions. Each molecule has been attached to two (111)-directed gold electrodes; one of these electrodes is pyramidal, while the other is a planar electrode. Then the molecules and the first layer of electrodes were allowed to relax again, yielding the optimal junction geometries as shown in Figure 7. These layers were then used to extend the gold electrodes to infinity. For each structure, the transmission coefficient $T(E)$ describing the propagation of electrons of energy E from the left to the right electrode was calculated by first obtaining the corresponding Hamiltonian and overlap matrices using SIESTA and then using the GOLLUM code to compute $T(E)$ via the relation $T(E) = \text{Tr}\{\Gamma_R(E) G^R(E) \Gamma_L(E) G^{R\dagger}(E)\}$; in this expression, $\Gamma_{L,R}(E) = i(\sum_{L,R}(E) - \sum_{L,R}^{\dagger}(E))$ describes the level broadening due to the coupling between left (L) and right (R) electrodes and the central scattering region, $\sum_{L,R}(E)$ is the retarded self-energy associated with this coupling, and $G^R = (ES - H - \sum_L - \sum_R)^{-1}$ is the retarded Green's function, where H is the Hamiltonian and S is the overlap matrix (both of them obtained from SIESTA). Finally the room-temperature electrical conductance G was computed from the formula

$$G = G_0 \int_{\infty}^{-\infty} dE \, T(E) \left(-\frac{df(E)}{dE}\right)$$

where $f(E) = [e^{\beta(E-E_F)} + 1]^{-1}$ is the Fermi function, $\beta = 1/k_B T$, E_F is the Fermi energy and $G_0 = (2e^2/h)$ is the quantum of conductance. Since the quantity $-(df(E)/dE)$ is a probability distribution peaking at $E = E_F$, with a width of the order $k_B T$, the above expression shows that G/G_0 is obtained by averaging $T(E)$ over an energy range of order $k_B T$ in the vicinity of $E = E_F$. It is well-known that the Fermi energy E_F^{DFT} predicted by DFT is not usually reliable, and therefore plots are shown of G/G_0 as a function of $E_F - E_F^{\text{DFT}}$. To determine E_F, we compared the predicted values of all molecules with the experimental values and chose a single common value of E_F which gave the closest overall agreement. This yielded a value of $E_F - E_F^{\text{DFT}} = -0.07$ eV, which is used in all theoretical results.

■ ASSOCIATED CONTENT

Ⓢ Supporting Information

The Supporting Information is available free of charge on the ACS Publications website at DOI: 10.1021/acs.organo-met.6b00472.

Crystallographic data (CIF)
All computed molecule Cartesian coordinates (XYZ)
STM conductance data (ZIP)

■ AUTHOR INFORMATION

Corresponding Authors
*E-mail for R.J.N.: nichols@liv.ac.uk.
*E-mail for C.J.L.: c.lambert@lancaster.ac.uk.
*E-mail for M.R.B.: m.r.bryce@durham.ac.uk.
*E-mail for P.J.L.: paul.low@uwa.edu.au.

Author Contributions
#These authors contributed equally to this work.

Notes
The authors declare no competing financial interest.

■ REFERENCES

(1) Zhang, J.; Kuznetsov, A. M.; Medvedev, I. G.; Chi, Q.; Albrecht, T.; Jensen, P. S.; Ulstrup, J. *Chem. Rev.* **2008**, *108*, 2737−2791.
(2) Nichols, R. J.; Haiss, W.; Higgins, S. J.; Leary, E.; Martin, S.; Bethell, D. *Phys. Chem. Chem. Phys.* **2010**, *12*, 2801.
(3) Kiguchi, M.; Kaneko, S. *Phys. Chem. Chem. Phys.* **2013**, *15*, 2253.
(4) Low, P. J. *Dalton Trans.* **2005**, 2821−2824.
(5) Rigaut, S. *Dalton Trans.* **2013**, *42*, 15859−15863.
(6) Park, J.; Pasupathy, A. N.; Goldsmith, J. I.; Chang, C.; Yaish, Y.; Petta, J. R.; Rinkoski, M.; Sethna, J. P.; Abruna, H. D.; McEuen, P. L.; Ralph, D. C. *Nature* **2002**, *417*, 722−725.
(7) Liang, W. J.; Shores, M. P.; Bockrath, M.; Long, J. R.; Park, H. *Nature* **2002**, *417*, 725−729.
(8) Albrecht, T.; Moth-Poulsen, K.; Christensen, J. B.; Guckian, A.; Bjornholm, T.; Vos, J. G.; Ulstrup, J. *Faraday Discuss.* **2006**, *131*, 265−279.

(9) Ricci, A. M.; Calvo, E. J.; Martin, S.; Nichols, R. J. *J. Am. Chem. Soc.* **2010**, *132*, 2494−2495.

(10) Ponce, J.; Arroyo, C. R.; Tatay, S.; Frisenda, R.; Gaviña, P.; Aravena, D.; Ruiz, E.; van der Zant, H. S. J.; Coronado, E. *J. Am. Chem. Soc.* **2014**, *136*, 8314.

(11) Li, J.-C.; Wu, J.-Z.; Gong, Z. *J. Phys. Chem. Lett.* **2014**, *5*, 1017−1021.

(12) Sakamoto, R.; Katagiri, S.; Maeda, H.; Nishihara, H. *Coord. Chem. Rev.* **2013**, *257*, 1493−1506.

(13) Davidson, R.; Liang, J. H.; Milan, D. C.; Mao, B.-W.; Nichols, R. J.; Higgins, S. J.; Yufit, D. S.; Beeby, A.; Low, P. J. *Inorg. Chem.* **2015**, *54*, 5487−5494.

(14) Aragonès, A. C.; Aravena, D.; Cerda, J. I.; Acís-Castillo, Z.; Li, H.; Real, J. A.; Sanz, F.; Hihath, J.; Ruiz, E.; Díez-Pérez, I. *Nano Lett.* **2016**, *16*, 218−226.

(15) Zotti, L. A.; Leary, E.; Soriano, M.; Cuevas, J. C.; Palacios, J. J. *J. Am. Chem. Soc.* **2013**, *135*, 2052−2055.

(16) Leary, E.; Van Zalinge, H.; Higgins, S. J.; Nichols, R. J.; de Biani, F. F.; Leoni, P.; Marchetti, L.; Zanello, P. *Phys. Chem. Chem. Phys.* **2009**, *11*, 5198−5202.

(17) Choi, B.; Capozzi, B.; Ahn, S.; Turkiewicz, A.; Lovat, G.; Nuckolls, C.; Steigerwald, M. L.; Venkataraman, L.; Roy, X. *Chem. Sci.* **2016**, *7*, 2701−2705.

(18) Sherif, S.; Rubio-Bollinger, G.; Pinilla-Cienfuegos, E.; Coronado, E.; Cuevas, J. C.; Agrait, N. *Nanotechnology* **2015**, *26*, 291001.

(19) Wang, W. Z.; Wu, Y.; Ismayilov, R. H.; Kuo, J. H.; Yeh, C. Y.; Lee, H. W.; Fu, M. D.; Chen, C. H.; Lee, G. H.; Peng, S. M. *Dalton Trans.* **2014**, *43*, 6229−6235.

(20) Tsai, C. S.; Liu, I. P. C.; Tien, F. W.; Lee, G. H.; Yeh, C. Y.; Chen, C. H.; Peng, S. M. *Inorg. Chem. Commun.* **2013**, *38*, 152−155.

(21) Chen, I. W. P.; Fu, M. D.; Tseng, W. H.; Yu, J. Y.; Wu, S. H.; Ku, C. J.; Chen, C. H.; Peng, S. M. *Angew. Chem., Int. Ed.* **2006**, *45*, 5814−5818.

(22) Mayor, M.; von Hanisch, C.; Weber, H. B.; Reichert, J.; Beckmann, D. *Angew. Chem., Int. Ed.* **2002**, *41*, 1183−1186.

(23) Schull, T. L.; Kushmerick, J. G.; Patterson, C. H.; George, C.; Moore, M. H.; Pollack, S. K.; Shashidhar, R. *J. Am. Chem. Soc.* **2003**, *125*, 3202−3203.

(24) Mahapatro, A. K.; Ying, J. W.; Ren, T.; Janes, D. B. *Nano Lett.* **2008**, *8*, 2131−2136.

(25) Schwarz, F.; Kastlunger, G.; Lissel, F.; Egler-Lucas, C.; Semenov, S. N.; Venkatesan, K.; Berke, H.; Stadler, R.; Lortscher, E. *Nat. Nanotechnol.* **2015**, *11*, 170−176.

(26) Schwarz, F.; Kastlunger, G.; Lissel, F.; Riel, H.; Venkatesan, K.; Berke, H.; Stadler, R.; Lortscher, E. *Nano Lett.* **2014**, *14*, 5932−5940.

(27) Lissel, F.; Schwarz, F.; Blacque, O.; Riel, H.; Lortscher, E.; Venkatesan, K.; Berke, H. *J. Am. Chem. Soc.* **2014**, *136*, 14560−14569.

(28) Sugimoto, K.; Tanaka, Y.; Fujii, S.; Tada, T.; Kiguchi, M.; Akita, M. *Chem. Commun.* **2016**, *52*, 5796−5799.

(29) Marques-Gonzalez, S.; Yufit, D. S.; Howard, J. A. K.; Martin, S.; Osorio, H. M.; Garcia-Suarez, V. M.; Nichols, R. J.; Higgins, S. J.; Cea, P.; Low, P. J. *Dalton Trans* **2013**, *42*, 338−341.

(30) Meng, F. B.; Hervault, Y. M.; Shai, Q.; Hu, B. H.; Norel, L.; Rigaut, S.; Chen, X. D. *Nat. Commun.* **2014**, *5*, 3023.

(31) Luo, L.; Benameur, A.; Brignou, P.; Choi, S. H.; Rigaut, S.; Frisbie, C. D. *J. Phys. Chem. C* **2011**, *115*, 19955−19961.

(32) Kim, B.; Beebe, J. M.; Olivier, C.; Rigaut, S.; Touchard, D.; Kushmerick, J. G.; Zhu, X. Y.; Frisbie, C. D. *J. Phys. Chem. C* **2007**, *111*, 7521−7526.

(33) Wen, H.-M.; Yang, Y.; Zhou, X.-S.; Liu, J.-Y.; Zhang, D.-B.; Wang, J.-Y.; Chen, Z.-N.; Tian, Z.-Q. *Chem. Sci.* **2013**, *4*, 2471−2477.

(34) Liu, K.; Wang, X. H.; Wang, F. S. *ACS Nano* **2008**, *2*, 2315−2323.

(35) Zhao, X. T.; Huang, C.; Gulcur, M.; Batsanov, A. S.; Baghernejad, M.; Hong, W.; Bryce, M. R.; Wandlowski, T. *Chem. Mater.* **2013**, *25*, 4340−4347.

(36) Komoto, Y.; Fujii, S.; Nakamura, H.; Tada, T.; Nishino, T.; Kiguchi, M. *Sci. Rep.* **2016**, *6*, 26606.

(37) Hong, W.; Manrique, D. Z.; Moreno-García, P.; Gulcur, M.; Mishchenko, A.; Lambert, C. J.; Bryce, M. R.; Wandlowski, T. *J. Am. Chem. Soc.* **2012**, *134*, 2292−2304.

(38) Martin, S.; Grace, I.; Bryce, M. R.; Wang, C. S.; Jitchati, R.; Batsanov, A. S.; Higgins, S. J.; Lambert, C. J.; Nichols, R. J. *J. Am. Chem. Soc.* **2010**, *132*, 9157−9164.

(39) Park, Y. S.; Whalley, A. C.; Kamenetska, M.; Steigerwald, M. L.; Hybertsen, M. S.; Nuckolls, C.; Venkataraman, L. *J. Am. Chem. Soc.* **2007**, *129*, 15768−15769.

(40) Kamenetska, M.; Quek, S. Y.; Whalley, A. C.; Steigerwald, M. L.; Choi, H. J.; Louie, S. G.; Nuckolls, C.; Hybertsen, M. S.; Neaton, J. B.; Venkataraman, L. *J. Am. Chem. Soc.* **2010**, *132*, 6817−6821.

(41) Kim, T.; Vazquez, H.; Hybertsen, M. S.; Venkataraman, L. *Nano Lett.* **2013**, *13*, 3358−3364.

(42) Saitner, M.; Eberle, F.; Baccus, J.; D'Olieslaeger, M.; Wagner, P.; Kolb, D. M.; Boyen, H.-G. *J. Phys. Chem. C* **2012**, *116*, 21810−21815.

(43) Davidson, R.; Al-Owaedi, O. A.; Milan, D. C.; Zeng, Q.; Tory, J.; Hartl, F.; Higgins, S. J.; Nichols, R. J.; Lambert, C. J.; Low, P. J. *Inorg. Chem.* **2016**, *55*, 2691−2700.

(44) Obersteiner, V.; Egger, D. A.; Zojer, E. *J. Phys. Chem. C* **2015**, *119*, 21198−21208.

(45) Ballesteros, L. M.; Martín, S.; Marques-Gonzalez, S.; Lopez, M. C.; Higgins, S. J.; Nichols, R. J.; Low, P. J.; Cea, P. *J. Phys. Chem. C* **2015**, *119*, 784−793.

(46) Wang, C.; Batsanov, A. S.; Bryce, M. R.; Martin, S.; Nichols, R. J.; Higgins, S. J.; Garcia-Suarez, V. M.; Lambert, C. J. *J. Am. Chem. Soc.* **2009**, *131*, 15647−15654.

(47) Moreno-Garcia, P.; Gulcur, M.; Manrique, D. Z.; Pope, T.; Hong, W. J.; Kaliginedi, V.; Huang, C. C.; Batsanov, A. S.; Bryce, M. R.; Lambert, C.; Wandlowski, T. *J. Am. Chem. Soc.* **2013**, *135*, 12228−12240.

(48) Haiss, W.; van Zalinge, H.; Higgins, S. J.; Bethell, D.; Hobenreich, H.; Schiffrin, D. J.; Nichols, R. J. *J. Am. Chem. Soc.* **2003**, *125*, 15294−15295.

(49) Capozzi, B.; Dell, E. J.; Berkelbach, T. C.; Reichman, D. R.; Venkataraman, L.; Campos, L. M. *J. Am. Chem. Soc.* **2014**, *136*, 10486−10492.

(50) (a) Becke, A. D. *J. Chem. Phys.* **1993**, *98*, 5648−5652. (b) Stephens, P. J.; Devlin, F. J.; Chabalowski, C. F.; Frisch, M. J. *J. Phys. Chem.* **1994**, *98*, 11623−11627.

(51) (a) Hay, P. J.; Wadt, W. R. *J. Chem. Phys.* **1985**, *82*, 270−283. (b) Wadt, W. R.; Hay, P. J. *J. Chem. Phys.* **1985**, *82*, 284−298. (c) Hay, P. J.; Wadt, W. R. *J. Chem. Phys.* **1985**, *82*, 299−310.

(52) (a) Petersson, G. A.; Bennett, A.; Tensfeldt, T. G.; Al-Laham, M. A.; Shirley, W. A.; Mantzaris, J. *J. Chem. Phys.* **1988**, *89*, 2193−2198. (b) Petersson, G. A.; Al-Laham, M. A. *J. Chem. Phys.* **1991**, *94*, 6081−6090.

(53) Marques-Gonzalez, S.; Parthey, M.; Yufit, D. S.; Howard, J. A. K.; Kaupp, M.; Low, P. J. *Organometallics* **2014**, *33*, 4947−4963.

(54) Georgiev, V. P.; McGrady, J. E. *J. Am. Chem. Soc.* **2011**, *133*, 12590−12599.

(55) Ferrer, J.; Lambert, C. J.; Garcia-Suarez, V. M.; Manrique, D. Z.; Visontai, D.; Oroszlany, L.; Rodriguez-Ferradas, R.; Grace, I.; Bailey, S. W. D.; Gillemot, K.; Sadeghi, H.; Algharagholy, L. *New J. Phys.* **2014**, *16*, 093029.

(56) Lambert, C. J. *Chem. Soc. Rev.* **2015**, *44*, 875−888.

(57) Markussen, T.; Settnes, M.; Thygesen, K. S. *J. Chem. Phys.* **2011**, *135*, 144104.

(58) Häkkinen, H. *Nat. Chem.* **2012**, *4*, 443−455.

(59) Mishchenko, A.; Zotti, L. A.; Vonlanthen, D.; Burkle, M.; Pauly, F.; Cuevas, J. C.; Mayor, M.; Wandlowski, T. *J. Am. Chem. Soc.* **2011**, *133*, 184−187.

(60) Quek, S. Y.; Kamenetska, M.; Steigerwald, M. L.; Choi, H. J.; Louie, S. G.; Hybertsen, M. S.; Neaton, J. B.; Venkataraman, L. *Nat. Nanotechnol.* **2009**, *4*, 230−234.

(61) Dell, E. J.; Capozzi, B.; Xia, J. L.; Venkataraman, L.; Campos, L. M. *Nat. Chem.* **2015**, *7*, 209−214.

(62) Fox, M. A.; Harris, J. E.; Heider, S.; Pérez-Gregorio, V.; Zakrzewska, M. E.; Farmer, J. D.; Yufit, D. S.; Howard, J. A. K.; Low, P. J. *J. Organomet. Chem.* **2009**, *694*, 2350−2358.

(63) Bailar, J. C., Jr.; Itatani, H. *Inorg. Chem.* **1965**, *4*, 1618−1620.

(64) Zhou, C.-Z.; Liu, T.; Xu, J.-M.; Chen, Z.-K. *Macromolecules* **2003**, *36*, 1457−1464.

(65) Haiss, W.; Lackey, D.; Sass, J. K.; Besocke, K. H. *J. Chem. Phys.* **1991**, *95*, 2193−2196.

(66) Dolomanov, O. V.; Bourhis, L. J.; Gildea, R. J.; Howard, J. A. K.; Puschmann, H. *J. Appl. Crystallogr.* **2009**, *42*, 339−341.

(67) Sheldrick, G. M. *Acta Crystallogr., Sect. A: Found. Crystallogr.* **2008**, *64*, 112−122.

(68) Frisch, M. J.; Trucks, G. W.; Schlegel, H. B.; Scuseria, G. E.; Robb, M. A.; Cheeseman, J. R.; Scalmani, G.; Barone, V.; Mennucci, B.; Petersson, G. A.; Nakatsuji, H.; Caricato, M.; Li, X.; Hratchian, H. P.; Izmaylov, A. F.; Bloino, J.; Zheng, G.; Sonnenberg, J. L.; Hada, M.; Ehara, M.; Toyota, K.; Fukuda, R.; Hasegawa, J.; Ishida, M.; Nakajima, T.; Honda, Y.; Kitao, O.; Nakai, H.; Vreven, T.; Montgomery, J. A.; Peralta, J. E.; Ogliaro, F.; Bearpark, M.; Heyd, J. J.; Brothers, E.; Kudin, K. N.; Staroverov, V. N.; Kobayashi, R.; Normand, J.; Raghavachari, K.; Rendell, A.; Burant, J. C.; Iyengar, S. S.; Tomasi, J.; Cossi, M.; Rega, N.; Millam, J. M.; Klene, M.; Knox, J. E.; Cross, J. B.; Bakken, V.; Adamo, C.; Jaramillo, J.; Gomperts, R.; Stratmann, R. E.; Yazyev, O.; Austin, A. J.; Cammi, R.; Pomelli, C.; Ochterski, J. W.; Martin, R. L.; Morokuma, K.; Zakrzewski, V. G.; Voth, G. A.; Salvador, P.; Dannenberg, J. J.; Dapprich, S.; Daniels, A. D.; Farkas, Ö.; Foresman, J. B.; Ortiz, J. V.; Cioslowski, J.; Fox, D. J. *Gaussian 09*, Revision D.01; Gaussian Inc., Wallingford, CT, 2009.

(69) O'Boyle, N. M.; Tenderholt, A. L.; Langner, K. M. *J. Comput. Chem.* **2008**, *29*, 839−845.

(70) Perdew, J. P.; Chevary, J. A.; Vosko, S. H.; Jackson, K. A.; Pederson, M. R.; Singh, D. J.; Fiolhais, C. *Phys. Rev. B: Condens. Matter Mater. Phys.* **1992**, *46*, 6671−6687.

■ NOTE ADDED AFTER ASAP PUBLICATION

In the version of this paper published on August 3, 2016, STM conductance data were inadvertently left out of the Supporting Information for this paper. In the version that appears on the web as of August 25, 2016, these data are given in the Supporting Information.